Lumped Element Modeling of Piezoelectric-Driven Synthetic Jet Actuators

Quentin Gallas,[1£] Jose Mathew,[1£] Anurag, Kasyap,[1£] Ryan Holman,[1£]
Toshikazu Nishida,[2¥], Bruce Carroll,[1†] Mark Sheplak,[1§] and Louis Cattafesta[1¶]

[1]Department of Aerospace Engineering, Mechanics, and Engineering Science
[2]Department of Electrical and Computer Engineering
University of Florida
Gainesville, Florida 32611-6250
(352) 846-3017, (352) 846-3028 (FAX), catman@aero.ufl.edu

Abstract

This paper presents a lumped element model of a piezoelectric-driven synthetic jet actuator. A synthetic jet, also known as a zero net mass-flux device, uses a vibrating diaphragm to generate an oscillatory flow through a small orifice or slot. In lumped element modeling (LEM), the individual components of a synthetic jet are modeled as elements of an equivalent electrical circuit using conjugate power variables. The frequency response function of the circuit is derived to obtain an expression for Q_{out}/V_{AC}, the volume flow rate per applied voltage. The circuit is analyzed to provide physical insight into the dependence of the device behavior on geometry and material properties. Methods to estimate the model parameters are discussed, and experimental verification is presented. In addition, the model is used to estimate the performance of two prototypical synthetic jets, and the results are compared with experiment.

1 Introduction

Synthetic jet actuators have been the focus of significant research activity for the past decade (Smith and Glezer 1998). The interest in synthetic jets is primarily due to their utility in flow control applications, such as separation control, mixing enhancement, etc. (Amitay et al. 1998; Smith et al. 1998; Chen et al. 1999; Honohan et al. 2000; Chatlynne et al. 2001).

A schematic of a synthetic jet actuator is shown in Figure 1. A typical synthetic jet, also known as a zero net mass-flux device, uses a vibrating diaphragm to drive oscillatory flow through a small orifice or slot. Although there is no source, a mean jet flow is established a few diameters from the orifice due to

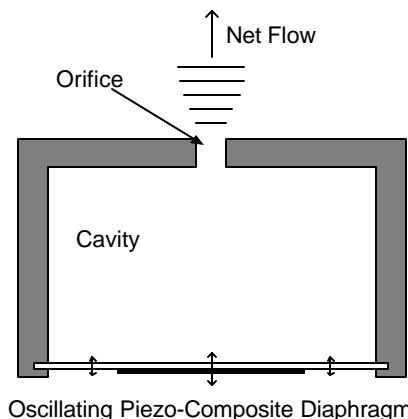the entrained fluid (in the absence of any grazing external flow).

Figure 1: Schematic of a Synthetic Jet.

In addition to studies that emphasize applications, there are numerous others that have concentrated on the design, visualization, and/or measurements of synthetic jets (Crook et al. 1999; Chen et al. 2000; Crook and Wood, 2001; Gilarranz and Rediniotis, 2001). Furthermore, several computational studies also have focused on fundamental aspects of these devices (Kral et al. 1997; Rizzeta et al. 1998; Mallinson et al. 2000; Utturkar et al. 2002). Crook and Wood (2001) emphasize the importance of understanding the scaling and operational characteristics of a synthetic jet. Clearly, this information is required for a user to design an appropriate device for a particular application. In addition, feedback control applications require the actuator transfer function that relates the input voltage to the output property of interest (e.g., volumetric flow rate) in the control system.

The design itself represents an electro-mechanical-acoustic coupled system with frequency dependent properties determined by device dimensions and material properties. The analysis and design of coupled-domain transducer systems are commonly performed using lumped element models (Fisher 1955; Hunt 1982; Rossi 1988).

The main assumption employed in LEM is that the characteristic length scales of the governing

---

[£] Graduate Student, Student Member AIAA

[¥] Associate Professor

[†] Associate Professor, Member AIAA

[¶] Assistant Professor, Senior Member AIAA

[§] Assistant Professor, Member AIAA

Report Documentation Page

Public reporting burden for the collection of information is estimated to average 1 hour per response, including the time for reviewing instructions, searching existing data sources, gathering and maintaining the data needed, and completing and reviewing the collection of information. Send comments regarding this burden estimate or any other aspect of this collection of information, including suggestions for reducing this burden, to Washington Headquarters Services, Directorate for Information Operations and Reports, 1215 Jefferson Davis Highway, Suite 1204, Arlington VA 22202-4302. Respondents should be aware that notwithstanding any other provision of law, no person shall be subject to a penalty for failing to comply with a collection of information if it does not display a currently valid OMB control number.

1. REPORT DATE **2002**	2. REPORT TYPE	3. DATES COVERED **00-00-2002 to 00-00-2002**

4. TITLE AND SUBTITLE	5a. CONTRACT NUMBER
Lumped Element Modeling of Piezoelectric-Driven Synthetic Jet Actuators	5b. GRANT NUMBER
	5c. PROGRAM ELEMENT NUMBER
6. AUTHOR(S)	5d. PROJECT NUMBER
	5e. TASK NUMBER
	5f. WORK UNIT NUMBER

7. PERFORMING ORGANIZATION NAME(S) AND ADDRESS(ES) **University of Florida,Department of Electrical and Computer Engineering,Gainesville,FL,32611**	8. PERFORMING ORGANIZATION REPORT NUMBER

9. SPONSORING/MONITORING AGENCY NAME(S) AND ADDRESS(ES)	10. SPONSOR/MONITOR'S ACRONYM(S)
	11. SPONSOR/MONITOR'S REPORT NUMBER(S)

12. DISTRIBUTION/AVAILABILITY STATEMENT
Approved for public release; distribution unlimited

13. SUPPLEMENTARY NOTES

14. ABSTRACT

15. SUBJECT TERMS

16. SECURITY CLASSIFICATION OF:			17. LIMITATION OF ABSTRACT	18. NUMBER OF PAGES **10**	19a. NAME OF RESPONSIBLE PERSON
a. REPORT **unclassified**	b. ABSTRACT **unclassified**	c. THIS PAGE **unclassified**			

physical phenomena are much larger than the largest geometric dimension. For example, in an acoustic system, the acoustic wavelength must be significantly larger than the device itself. If this assumption holds, then the governing partial differential equations for the distributed system can be "lumped" into a set of coupled ordinary differential equations. This approach provides a simple method to estimate the dynamic response of a synthetic jet for design and control-system implementation.

The purpose of this paper is to rigorously study the application of lumped-element modeling to piezoelectric-driven synthetic jet actuators. To the authors knowledge, this represents the first application of LEM to piezoelectric-driven synthetic jets. McCormick (2000) employed LEM to a speaker-driven synthetic jet, while Rathnasingham and Breuer (1997) were the first to develop a low-order model of a synthetic jet. In this paper, the various lumped elements for each component of a synthetic jet are theoretically developed. The resulting equivalent circuit is then analyzed to understand the effects of geometry and material properties on important design parameters, such as resonance frequency and volume displacement per applied voltage. The model assumptions and limitations are discussed, along with the results of an ongoing experimental study designed to quantify the validity of this modeling approach.

2   Lumped Element Model

In LEM, the coupling between the various energy domains is realized via simplified device representations connected to form equivalent circuits. The equivalent circuit model is constructed by lumping the distributed energy storage and dissipation into ideal generalized circuit elements. In this electroacoustic analogy, pressure and voltage are effort variables, while current and volumetric flow rate are flow variables. For this paper, we employ an impedance analogy, in which elements that share a common effort are connected in parallel, while those sharing a common flow are connected in series. For a synthetic jet, three different energy domains are involved: electrical, mechanical, and fluidic/acoustic.

The electromechanical actuator consists of a clamped axisymmetric PZT patch bonded to a metal diaphragm. The composite diaphragm is driven into motion via an applied AC voltage. The primary purpose of the piezoelectric diaphragm is to produce large volume displacements in order to draw fluid into and out of the cavity. This represents a conversion from the mechanical to acousto-fluidic domain. Consequently, we focus on the first axisymmetric vibration mode of the composite diaphragm (see Prasad et al. 2002 for details of this analysis). Specifically, linear composite plate theory is used to obtain the short-circuit pressure-deflection characteristics. Then, the diaphragm is lumped into an equivalent acoustic mass and acoustic compliance. The former represents stored kinetic energy, and the latter stored potential energy.

In general, the cavity contains a compressible gas that stores potential energy and is therefore modeled as an acoustic compliance. Finally, viscous effects in the orifice dissipate a portion of the kinetic energy stored in the motion of the oscillating fluid mass. Therefore, there will be an effective acoustic mass and acoustic resistance associated with the orifice neck. Flow through the orifice also produces losses associated with the discharge of flow from the jet exit. In addition, for low operational frequencies where $ka_o = wa_o/c_0 \ll 1$ (where a_o is the orifice radius and c_0 is the speed of sound), an acoustic radiation mass also be added if the orifice is ejecting into a semi-infinite medium (Rossi 1988).
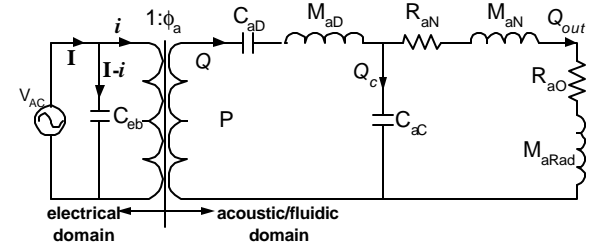

Figure 2: Equivalent circuit representation of a piezoelectric-driven synthetic jet.

The equivalent circuit representation for the synthetic jet is shown in Figure 2. In the notation below, the first subscript denotes the domain (e.g., "a" for acoustic and "e" for electric), and the second subscript describes the element (e.g., "D" for diaphragm). In the electrical domain, C_{eb} is the blocked electrical capacitance of the piezoelectric diaphragm driven by an AC voltage V_{AC}. The term blocked is used since it is the impedance seen by the source when the diaphragm motion is prevented.

In the acoustic domain, C_{aD} and M_{aD} are the acoustic compliance and mass of the piezoceramic composite diaphragm, respectively. M_{aD} may include a radiation mass, if appropriate. Although not shown, an acoustic resistance could also be included in series with C_{aD} and M_{aD} to model structural damping effects. C_{aC} is the acoustic compliance of the cavity, while R_{aN} and M_{aN} are the acoustic resistance and mass of the fluid in the neck, respectively. Finally, R_{aO} is the resistance associated with the orifice discharge, and M_{aRad} is the acoustic radiation mass of the orifice.

In this paper, we assume that the synthetic jet exhausts into a semi-infinite ambient air medium, and that the diaphragm is not subject to a mean differential pressure. If necessary, a vent channel can be used to equilibrate the mean static pressure across the diaphragm, in a manner similar to a microphone (Sheplak et al. 1998). For simplicity, we will assume that there is no grazing flow and neglect nonlinear amplitude and compressibility effects in the orifice.

The structure of the equivalent circuit is explained as follows. An AC voltage V_{AC} is applied across the piezoceramic to create an effective acoustic pressure that drives the diaphragm into motion. This represents a conversion from the electrical to the acoustic domain and is accounted for via a transformer with a turns ratio $\boldsymbol{f}_a$ with units of [Pa/V]. An ideal transformer (i.e., power conserving) converts energy from one domain to another and obeys the relations

$$i = \boldsymbol{f}_a Q \text{ and } V_{AC} = \frac{P}{\boldsymbol{f}_a}. \qquad \{1\}$$

In addition, a transformer converts an electrical impedance Z_e to an acoustic impedance Z_a via

$$Z_e = \frac{V_{AC}}{i} = \frac{P/\boldsymbol{f}_a}{\boldsymbol{f}_a Q} = \frac{P/Q}{\boldsymbol{f}_a^2} = \frac{Z_a}{\boldsymbol{f}_a^2}. \qquad \{2\}$$

The motion of the diaphragm can either compress the fluid in the cavity or can eject/ingest fluid through the orifice. Physically, this is represented as a volume velocity divider, $Q = Q_c + Q_{out}$. The goal of the design is to maximize the magnitude of the volume flow rate through the orifice per applied voltage $|Q_{out}/V_{AC}|$.

3 Equivalent Circuit Model Analysis

Before estimating the lumped parameters defined above, it is instructive to analyze the equivalent circuit to obtain the frequency response function $Q_{out}(s)/V_{AC}(s)$, where $s = j\boldsymbol{w}$. Using Eq. {2}, the transformer can be eliminated by converting each of the acoustic impedances to their electrical equivalent. The result is depicted in Figure 3, where

$$Z_{eD}(s) = \frac{1}{\boldsymbol{f}_a^2}\left(sM_{aD} + \frac{1}{sC_{aD}}\right),$$

$$Z_{eC}(s) = \frac{1}{\boldsymbol{f}_a^2}\left(\frac{1}{sC_{aC}}\right), \text{ and} \qquad \{3\}$$

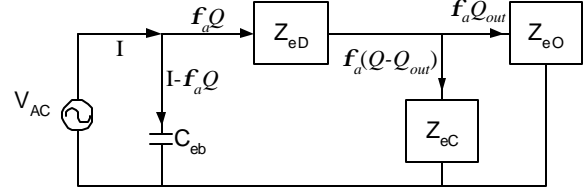$$Z_{eO}(s) = \frac{\left[(R_{aN} + R_{aO}) + s(M_{aN} + M_{aRad})\right]}{\boldsymbol{f}_a^2}.$$

Figure 3: Alternative equivalent circuit model.

Substituting in the expressions for $Z_{eD}, Z_{eC},$ and Z_{eO} and grouping powers of s in the numerator and denominator results in

$$\frac{Q_{out}(s)}{V_{AC}(s)} = \frac{\boldsymbol{f}_a C_{aD} s}{a_4 s^4 + a_3 s^3 + a_2 s^2 + a_1 s + 1}. \qquad \{4\}$$

where

$$\begin{aligned} a_1 &= (R_{aO} + R_{aN})(C_{aD} + C_{aC}), \\ a_2 &= (M_{aRad} + M_{aN})(C_{aD} + C_{aC}) + M_{aD}C_{aD}, \\ a_3 &= C_{aC}M_{aD}C_{aD}(R_{bO} + R_{aN}), \text{ and} \\ a_4 &= C_{aC}M_{aD}C_{aD}(M_{aRad} + M_{aN}). \end{aligned} \qquad \{5\}$$

Although this expression is complex, it reveals some important features without having to estimate any of the parameters in Eq. {5}. For the purposes of this discussion, these parameters can be thought of as constants, although in reality some are likely to exhibit some frequency and amplitude dependence (i.e., due to nonlinear effects). For a DC voltage ($s = 0$), the volume velocity is zero. At low frequencies ($s \rightarrow 0$), the volume velocity is proportional to $d_a V_{AC} \boldsymbol{w}$ since the transduction factor is defined as $\boldsymbol{f}_a = d_a/C_{aD}$, where d_a is an effective acoustic piezoelectric constant defined in Eq. {19}. This result emphasizes the need to optimize the design of the piezoceramic composite diaphragm (Prasad et al. 2002).

At high frequencies ($s \rightarrow \infty$), we find that

$$\frac{Q_{out}}{V_{AC}} = \frac{d_a}{C_{aC}C_{aD}M_{aD}(M_{aN} + M_{aRad})s^3}. \qquad \{6\}$$

The output therefore decreases at a rate of 60 dB/decade and is inversely proportional to the masses and compliances in the system.

The denominator in Eq. {4} is a 4th-order polynomial in s, indicating two resonance frequencies. It is difficult to obtain a compact analytical expression for the two resonance frequencies (Fischer 1955). However, the resonance frequencies, $f_{1,2}$, are controlled by the piezoelectric

diaphragm natural frequency f_D and the Helmholtz frequency of the cavity f_C

$$f_D = \frac{1}{2\pmb{p}} \sqrt{\frac{1}{M_{aD}C_{aD}}}$$

$$f_C = \frac{1}{2\pmb{p}} \sqrt{\frac{1}{\left(M_{aN}+M_{aRad}\right)C_{aC}}}$$ {7}

with the constraint that

$$f_1 f_2 = f_D f_C . \qquad \{8\}$$

To gain physical insight into the behavior of the device, three important cases are examined below.

3.1   Case I: Incompressible Limit $\frac{C_{aC}}{C_{aD}} \to 0$

Assuming that the fluid is an ideal gas, then the acoustic cavity compliance, which is analogous to the inverse of the gas spring constant, is obtained from the cavity volume V_0, gas density $\pmb{r}_0$, and the speed of sound c_0 via

$$C_{aC} = \frac{V_0}{\pmb{r}_0 c_0^{\ 2}} . \qquad \{9\}$$

In practice, $C_{aC}/C_{aD} \to 0$ is achieved by minimizing the cavity volume or operating in a liquid medium.

Since the coefficients a_3 and a_4 in Eq. {5} are both proportional to C_{aC}, the synthetic jet transfer function reduces to the 2$^\text{nd}$-order system

$$\frac{Q_{out}\left(s\right)}{V_{AC}\left(s\right)} = \frac{\dfrac{d_a}{a_2'}s}{s^2 + \dfrac{a_1'}{a_2'}s + \dfrac{1}{a_2'}} , \qquad \{10\}$$

where the prime denotes the limit with $C_{aC}/C_{aD} \to 0$.

Eq. {10} is written in the form of a canonical 2$^\text{nd}$-order system $s^2 + 2\pmb{z}\pmb{w}_n s + \pmb{w}_n^2$. By inspection, we find that the natural frequency and damping ratio for the incompressible case are given by

$$\pmb{w}_{incomp} = \sqrt{\dfrac{1}{C_{aD}M_{aD}\left(1+\dfrac{M_{aN}+M_{aRad}}{M_{aD}}\right)}} \qquad \{11\}$$

and

$$\pmb{z}_{incomp} = \frac{1}{2}\left(R_{aO}+R_{aN}\right)\sqrt{\frac{C_{aD}}{M_{aN}+M_{aRad}+M_{aD}}} . \{12\}$$

If $M_{aD} \gg M_{aN}+M_{aRad}$, then the natural frequency of the synthetic jet actuator equals that of the diaphragm. At resonance, the response is limited by the flow resistances in the orifice and the acoustic compliance of the diaphragm

$$\frac{Q_{out}}{V_{AC}} = \frac{1}{C_{aD}}\frac{d_a}{R_{aO}+R_{aN}} . \qquad \{13\}$$

3.2   Case II: Rigid Diaphragm Limit $\frac{C_{aD}}{C_{aC}} \to 0$

As described in Prasad et al. (2002), the size of the piezoceramic patch is not negligible compared to the metal diaphragm for high actuation performance. In this case, the piezoceramic composite diaphragm *cannot* be accurately modeled as a homogeneous circular plate. Nonetheless, assuming that the diaphragm is clamped, the acoustic compliance of a homogeneous clamped circular plate provides insight into the scaling behavior of the diaphragm

$$C_{aD} = \frac{\pmb{p} a^6 \left(1-\pmb{n}^2\right)}{16Eh^3} , \qquad \{14\}$$

where a is the radius, E is the elastic modulus, $\pmb{n}$ is Poisson's ratio, and h is the thickness. From Eq. {14}, C_{aD} decreases with decreasing thickness ratio a/h and increasing elastic modulus.

As in the previous case, the coefficients a_3 and a_4 in Eq. {5} are zero, and the synthetic jet transfer function reduces to a 2$^\text{d}$-order system. The limit $C_{aD}/C_{aC} \to 0$ leads to the following expressions for the natural frequency, damping ratio, and response at resonance:

$$\pmb{w}_{stiff} = \sqrt{\dfrac{1}{\left(M_{aN}+M_{aRad}\right)C_{aC}}} , \qquad \{15\}$$

$$\pmb{z}_{stiff} = \frac{1}{2}\left(R_{aO}+R_{aN}\right)\sqrt{\frac{C_{aC}}{M_{aRad}+M_{aD}}} , \qquad \{16\}$$

and

$$\frac{Q_{out}}{V_{AC}} = \frac{1}{C_{aC}}\frac{d_a}{R_{aO}+R_{aN}} . \qquad \{17\}$$

In this case, the natural frequency of the jet corresponds to the Helmholtz frequency.   At resonance, the response is limited by the flow resistances in the orifice and the acoustic compliance of the cavity.   By comparing with Eq. {13}, the resonant response differs for these cases by the ratio of the acoustic compliances.

3.3 Case III: Equal Resonant Frequencies $f_1 = f_2$

One other case of interest occurs when the two natural frequencies are equal to each other, $f_1 = f_2$. However, this does not imply that $f_D = f_C$, as seen in Eq. {8}. It can be shown that in this case, the following is true:

$$\frac{C_{aC}}{C_{aD}} + \frac{C_{aD}}{C_{aC}} + 2 = \frac{M_{aD}}{M_{aN} + M_{aRad}} \ . \qquad \{18\}$$

The cavity volume can thus be adjusted accordingly to provide a single dominant peak with large resonant response $\left| Q_{out}/V_{AC} \right|$.

4 Model Parameter Estimation

In this section, we outline the methods and assumptions used to estimate each of the quantities in Eq. {5}. The interested reader is referred to Rossi (1988) and Beranek (1993) for details of the methodology.

The piezoelectric diaphragm vibrates in response to both an applied AC voltage and oscillatory differential pressure according to the relation

$$Q = j\boldsymbol{w}\left(d_a V_{AC} + C_{aD}P\right). \qquad \{19\}$$

Here $d_a = \left|\left(Q/j\boldsymbol{w}V_{AC}\right)\right|_{P=0}$ is the effective acoustic piezoelectric constant that relates the volume velocity of the diaphragm to the applied voltage V_{AC}. $C_{aD} = \left(Q/j\boldsymbol{w}P\right)\big|_{V_{AC}=0} = \left(\Delta Volume/P\right)\big|_{V_{AC}=0}$ relates an applied differential pressure to the volume change of the diaphragm.

The vertical deflection $w(r)$ due to an applied differential pressure is also lumped into an equivalent acoustic mass M_{aD} by equating the lumped kinetic energy of the vibrating diaphragm to the total kinetic energy using

$$\frac{1}{2}M_{aD}Q^2 = \int_0^a \frac{\boldsymbol{r}'(r)}{2}\dot{w}(r)^2 \, 2\boldsymbol{p}\, r dr, \qquad \{20\}$$

where $\boldsymbol{r}'(r)$ is the distributed mass per unit area, Q is the net volume velocity of the diaphragm, and $\dot{w}(r) = j\boldsymbol{w}w(r)$ is the distributed vertical velocity. All of these parameters are calculated via linear composite plate theory (see Prasad et al. 2002 for details).

The acoustic resistance of the neck is obtained assuming fully-developed laminar pipe flow in the neck of length L and radius a_0

$$R_{aN} = \frac{\Delta P_{out}}{Q_{out}} = \frac{8\boldsymbol{m}L}{\boldsymbol{p}\,a_0^{\,4}}\ , \qquad \{21\}$$

where $\boldsymbol{m}$ is the viscosity of the fluid and Q_{out} is the volume flow rate produced by the pressure ΔP_{out}.

Using the same assumption of fully-developed pipe flow, the acoustic mass in the neck is obtained from

$$\frac{1}{2}M_{aN}Q_{out}^2 = \frac{1}{2}\boldsymbol{r}_0 L \int_0^{a_0} u_0^2 \left[1 - \left(\frac{r}{a_0}\right)^2\right]^2 2\boldsymbol{p}\, r dr \quad \{22\}$$

or

$$M_{aN} = \frac{4\boldsymbol{r}_0 L}{3\boldsymbol{p}\,a_0^{\,2}} \qquad \{23\}$$

As mentioned above, the acoustic radiation mass M_{aRad} can be modeled, to first order, as a piston in an infinite baffle if the circular orifice is mounted in a plate that is much larger in extent than the orifice radius

$$M_{aRad} = \frac{8\boldsymbol{r}_0}{3\boldsymbol{p}^2 a_0}\ . \qquad \{24\}$$

The acoustic resistance associated with the discharge from the orifice can be approximated by modeling the orifice as a generalized Bernoulli flow meter (White 1979; McCormick 2000):

$$R_{aO} = \frac{\dfrac{1}{2}K_D\,\boldsymbol{r}_0\bar{u}}{\boldsymbol{p}\,a_0^2} = \frac{\dfrac{1}{2}K_D\,\boldsymbol{r}_0 Q_{out}}{\boldsymbol{p}^2 a_0^4}\ , \qquad \{25\}$$

where $\bar{u}$ is the mean velocity, and $K_D \approx O(1)$ is a nondimensional loss coefficient that is a function of orifice geometry, Reynolds number, and frequency. Note that R_{aO} is a function of the volume flow rate Q_{out} through the orifice and thereby represents a nonlinear resistance.

As mentioned above, a transduction factor is required to move from the electrical to the acoustic domain. This factor is given by

$$\boldsymbol{f}_a = \frac{d_a}{C_{aD}}\ . \qquad \{26\}$$

The blocked electrical capacitance C_{eb} in Figure 2 is related to the free electrical capacitance of the piezoceramic $C_0 = \boldsymbol{e}A_p / h_p$ by

$$C_{eb} = C_0\left(1-k^2\right) = C_0\left(1-\frac{d_a^2}{C_0 C_{aD}}\right), \qquad \{27\}$$

where k^2 is the electroacoustic coupling factor, e is the dielectric constant, A_p is the piezoceramic area, and h_p is the thickness of the piezoceramic.

The next section describes experiments designed to isolate and measure these parameters. This allows us to evaluate the effectiveness and limitations of the lumped element model.

5   Model Validation

A modular piezoelectric-driven synthetic jet was constructed, as shown in Figure 4, to perform a series of experiments to test the validity of the lumped element model parameters. The modular design permits a parametric study of the cavity volume, orifice diameter and length, and piezoelectric diaphragm diameter. In addition, an access hole is provided for a microphone to monitor the fluctuating pressure inside the cavity.
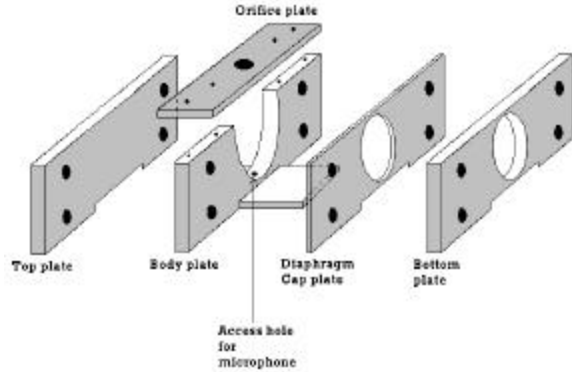

Figure 4: Assembly diagram of modular synthetic jet.

5.1   Piezoelectric Transduction

The first experiment tested the linear composite plate theory that provides estimates for C_{aD}, M_{aD}, and d_a. This was accomplished by measuring the velocity of the clamped vibrating diaphragm (excited by V_{AC}) using a scanning laser vibrometer and integrating the velocity to displacement in the frequency domain. The clamped circular diaphragm was removed from the synthetic jet apparatus and mounted on an optical table. The test was also performed in a vacuum chamber to eliminate fluid loading effects.

Table 1 provides the dimensions and material properties of the diaphragms. Figure 5(a) shows a comparison between the predicted and measured response of the piezoceramic diaphragm to a

sinusoidal excitation voltage at $f = 100$ Hz. The measured natural frequency of the diaphragm was ~2100 Hz while the computed resonance frequency was ~2800 Hz. The non-zero displacement at $r/a \approx 1$ in Figure 5(a) reveals a compliant boundary that does not achieve the "clamped" boundary condition assumed in the theory. When another diaphragm was tested using a separate mounting system and properly clamped, the agreement between theory and experiment was excellent, as shown in Figure 5(b). The measured and predicted natural frequencies agreed to within 2%.

Table 1: Piezoceramic Diaphragm Details.

Shim (Brass)	I	II
Elastic Modulus (Pa)	8.963×10^{10}	
Poisson's ratio	0.324	
Density (kg/m^3)	8700	
Thickness (mm)	0.20	0.10
Diameter (mm)	23.5	37
Piezoceramic (PZT-5A)		
Elastic Modulus (Pa)	6.1×10^{10}	
Poisson's ratio	0.33	
Density (kg/m^3)	7500	
Thickness (mm)	0.11	0.10
Diameter (mm)	20.5	25.0
Dielectric Permittivity (F/m)	8.85×10^{-12}	
d_{31} (m/V)	-2.7×10^{-10}	
C_{aD} (s^2.m^4/kg)	6.53×10^{-13}	2.23×10^{-11}
M_{aD} (kg/m^4)	8.15×10^3	2.43×10^3
φ_a (Pa/V)	88.6	15.1

Future testing will assess the severity of nonlinear effects when the excitation amplitude is increased. We will also seek to directly measure the acoustic compliance of the diaphragm C_{aD} in a normal incidence plane-wave tube.
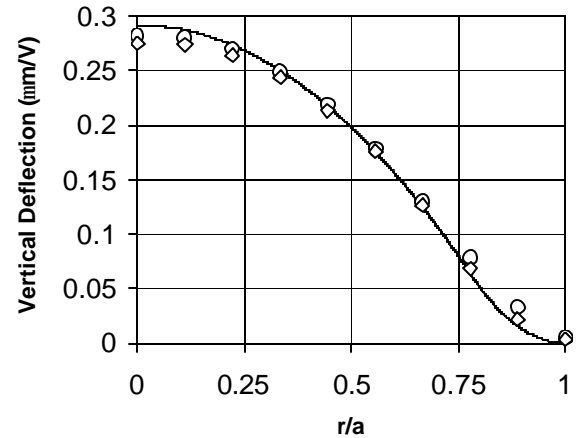
(a) Compliant boundary case.
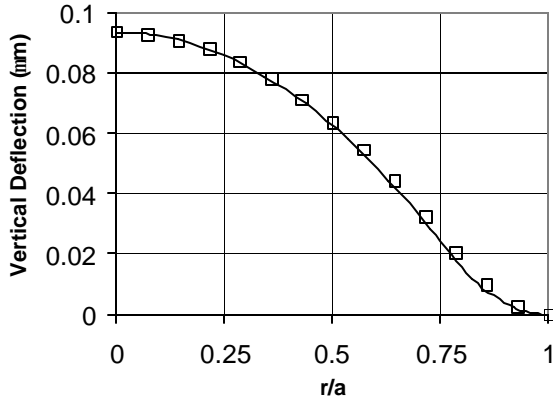
(b) Clamped boundary case.

Figure 5: Comparison between predicted and measured response of piezoceramic diaphragms to a sinusoidal excitation voltage at low frequency. Theory (—) and scanning laser vibrometer in ambient air (○, •) and in a vacuum chamber (◇).

5.2 Cavity Acoustic Compliance

The value for the cavity acoustic compliance C_{aC} is obtained from Eq. {9}. The cavity volume can be calculated from the geometry. To test the theory, the orifice was replaced with a solid cap to provide a closed cavity and all leaks were carefully minimized. The piezoceramic was then driven with a sinusoid, and the displacement of the vibrating diaphragm was measured with a laser displacement sensor. A B&K 1/8 in. microphone then measured the fluctuating pressure in the closed cavity.
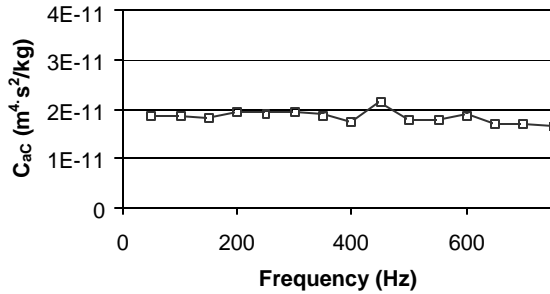

Figure 6: Measured acoustic compliance C_{aC} vs. frequency in closed cavity of synthetic jet.

The amplitude of the sinusoid was adjusted to avoid harmonics in either signal. The frequency response function between the pressure and displacement signal at the diaphragm center w_0 was used to measure P/w_0 at several frequencies and calculate C_{aC}, as shown in Figure 6. Using the average measured value of 9.89 MPa/m and the measured mode shape, the cavity volume was

determined to be 2.6×10^{-6} m³. This is within 4% of the cavity volume calculated from the geometric drawings.

5.3 Acoustic Mass and Resistance in Orifice

The flow in the neck of the orifice is modeled as a steady, fully-developed laminar flow in a circular duct of radius a_0 and length L. The resulting Poiseuille flow leads to the expressions for acoustic resistance and acoustic mass defined in Eqs. {21} and {23}, respectively. At higher frequencies, the velocity for the case of flow in a circular channel driven by an oscillating pressure gradient is discussed in White (1974)

$$u(r,t) = j\frac{\Delta P_{out}}{wr_0 L}\left\{1 - \frac{J_0\left(\sqrt{-j\dfrac{wr^2}{n}}\right)}{J_0\left(\sqrt{-j\dfrac{wa_0^2}{n}}\right)}\right\}e^{jwt} , \quad \{28\}$$

where J_0 is a Bessel function of zero order, and n is the kinematic viscosity. The velocity u is proportional to the pressure gradient and inversely proportional to $r_0 w$. Furthermore, the velocity profile is characterized by the Stokes number $St = \sqrt{wa_0^2/n}$. In the limit of $St \to 0$, the velocity profile asymptotes to a parabolic shape (i.e., Poiseuille flow). As St increases, the thickness of the Stokes layers decreases below a_0, leading to an inviscid core surrounded by a viscous annular region.
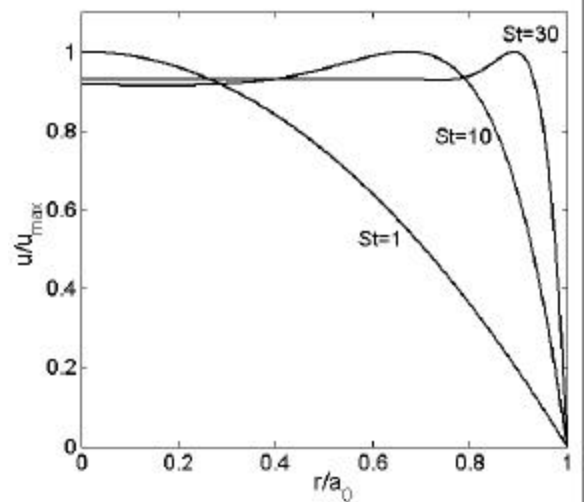

Figure 7: Variation in velocity profile vs. Stokes number $St = 1, 10,$ and 30 for oscillatory channel flow in a circular duct.

These velocity profiles can be integrated numerically to obtain Q_{out} and obtain the real

7

(resistive) and imaginary (reactive) parts of the acoustic impedance as a function of the Stokes number

$$\frac{\Delta P_{out}}{Q_{out}} = Z_{aN} = R_{aN} + jX_{aN} = R_{aN} + jwM_{aN} . \quad \{29\}$$

The results shown in Figure 8 reveal that, at low frequencies, the acoustic resistance asymptotes to the steady value given in Eq. {21} and increases gradually with frequency. However, the acoustic *mass* is approximately constant with frequency. The data in Figure 8 can be used to provide frequency dependent estimates for the acoustic resistance and mass in the lumped element model.
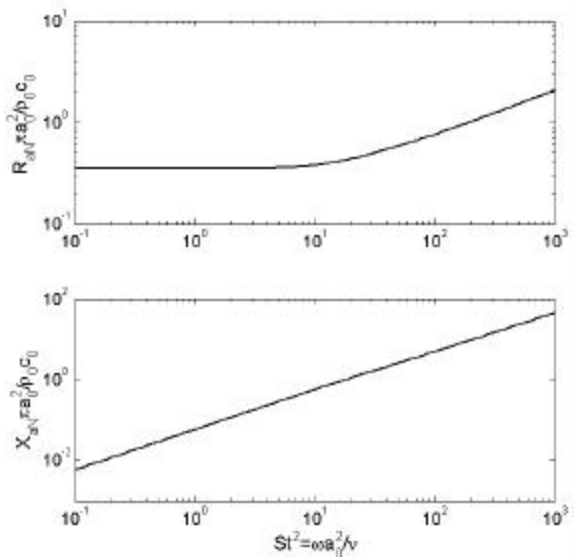

Figure 8: Nondimensional resistance and reactance vs. St^2 for oscillatory channel flow in a circular duct.

It should also be noted that, depending on the aspect ratio L/a_0 of the orifice, the fully developed assumption may not be valid. Only for large values of L/a_0 is the fully-developed assumption expected to be reasonable. For small values of L/a_0, the orifice loss given in Eq. {25} is expected to dominate.

The models discussed in this section are simple and neglect potentially significant issues, such as nonlinear effects due to large amplitude pressure oscillations in the cavity (Ingard 1967) and transition to turbulent flow and compressibility effects in the orifice. The grazing flow effects, which are relevant when the synthetic jet interacts with a boundary layer, have also been ignored (Mittal et al. 2001).

5.4   Comparison between Model & Experiment

In this section, the lumped element model is used to predict the performance of two synthetic jets vs.

frequency. The dimensions of the device are summarized in Tables 1 and 2.

A Dantec two-component Laser Doppler Velocimeter (LDV) system was used to measure the magnitude of the peak velocity produced by the synthetic jet vs. frequency. The synthetic jet was placed inside a large glass fish tank, which was filled with oil seed particles and closed. The probe volume was located over the center of the orifice as close as possible to the exit plane. The system was operated in backscatter mode and resulted in a probe-volume length that was larger than the diameter of the orifice. Because of the poor spatial resolution, the peak velocity in the jet was measured using a phase-averaging scheme.

Table 2: Synthetic Jet Details.

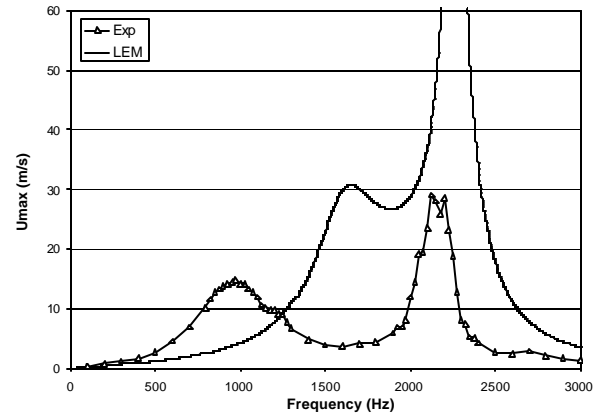| Cavity:	I	II
Volume (m^3)	2.50×10^{-6}	5.00×10^{-6}
Orifice:		
Radius (mm)	1.65	0.84
Length (mm)	1.65	0.84

Figure 9: Comparison between the lumped element model and experiment for Case I.

Case I uses a smaller piezoceramic diaphragm and cavity volume and a larger orifice than Case II. However, both devices use an orifice with the same aspect ratio L/a_0 and are driven with $V_{AC} = 50$ V amplitude sinusoids. The model prediction in Figure 9 has the correct shape, but the frequency of the first resonance peak is high. Furthermore, the velocities are overpredicted. Note that the peak velocity is estimated from Poiseuille flow, where $u_{max} = 2\overline{u} = 2Q_{out}/\left(p\,a_0^2\right)$. Since this relation is only valid at low frequencies for ducts with fully-developed flow, this approximation is likely to introduce significant error as frequency increases. Eq. {28} can be used to determine the relationship between u_{max} and Q_{out}, but this has not been done in

this paper. Clearly, the velocity profile must be measured and integrated to obtain Q_{out}.

Case II corresponds approximately to the situation described in Section 3.3. In particular, this combination brings the two resonance peaks close together, resulting in a single dominant peak with jet velocities of over 60 m/s. The lumped element model accurately predicts the resonance frequency and maximum velocity and also possesses the proper shape of the frequency response function.
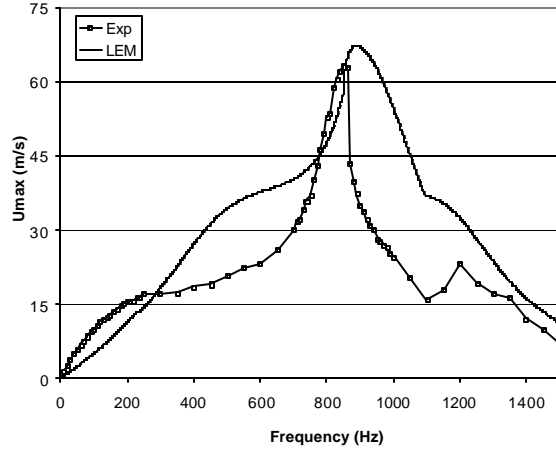

Figure 10: Comparison between the lumped element model and experiment for Case II.

These results reveal the power and shortcomings of the model in its present form. Clearly, the flow in the vicinity of the orifice must be studied further in order to obtain better estimates of the losses and velocity profile characteristics. Furthermore, from Figure 8 we expect the resistance to increase with frequency, but the current model only uses the DC value in Eq. {21}. Furthermore, the loss coefficient K_D in Eq. {25} is treated as a constant but is probably a function of (at least) the orifice Reynolds number, Stokes number, and geometry.

6   Conclusions and Future Work

A lumped element model of a piezoelectric-driven synthetic jet actuator has been developed and compared with experiment. LEM provides a compact analytical model and valuable physical insight into the dependence of the device behavior on geometry and material properties. The model reveals that a synthetic jet is a 4th-order coupled oscillator. One oscillator is a Helmholtz resonator, and the second is the piezoelectric diaphragm. Simple arguments reveal three important special cases corresponding to single oscillators. One case occurs when the fluid is incompressible (i.e. water) or, in the case of a gaseous medium, the acoustic compliance of the cavity is small compared to that of the piezoelectric diaphragm. The second case is similar

to that of a rigid piston and occurs when the acoustic compliance of the piezoelectric diaphragm is small compared to that of the cavity. In this case, the synthetic jet acts like a driven Helmholtz resonator. The third case occurs when the cavity compliance is adjusted to provide a single resonant peak as described in Eq. {18}.

Methods to estimate the parameters of the lumped element model were discussed in some detail and experiments were performed to isolate different components of the model and evaluate their suitability. The results indicate that the linear composite plate theory is accurate when the assumed clamped boundary condition is achieved. Similarly, the cavity acoustic compliance model was validated.

The details of the flow in the orifice requires further study. It is this region that dictates the acoustic mass and resistance in the neck. Accurate knowledge of the acoustic mass is required to determine the Helmholtz frequency of the synthetic jet, while the resistance limits the response of the device near resonance.

The model was applied to two prototypical synthetic jets and found to provide fair agreement with the measured performance. Better models are needed for the unsteady flow in the orifice, including that of entrance and exit effects. In addition, nonlinear and grazing flow effects remain to be studied in a rigorous fashion.

In future work, additional parameters will be varied in these experiments to yield a performance database for the synthetic jet. Emphasis will be placed on the ratio of the orifice length to the hole radius. This variable will be systematically varied in concert with the other important nondimensional parameters, such as the orifice Reynolds and the Stokes numbers. Additional velocity measurements with improved spatial resolution will also be performed to map out the spatial variations in the synthetic jet velocity field. Finally, an optimization study of the entire lumped element model is underway and should lead to synthetic jets with improved performance.

7   Acknowledgments

8   References

Amitay, M., Smith, B. L., and Glezer, A., "Aerodynamic Flow Control Using Synthetic Jet Technology," AIAA Paper 98-0208, Jan. 1998.

Beranek, L. L. Acoustics, Acoustic Society of America, Woodbury, NY, pp. 47-77, 1993.

Chatlynne, E., Rumigny, N., Amitay, M., and Glezer, A., "Virtual Aero-Shaping of a Clark-Y Airfoil Using Synthetic Jet Actuators," AIAA Paper 2001-0732, Jan. 2001.

Chen, F.-J., Yao, C., Beeler, G. B., Bryant, R. G., and Fox, R. L., "Development of Synthetic Jet Actuators for Active Flow Control at NASA Langley," AIAA Paper 2000-2405, June 2000.

Chen, Y., Liang, S., Aung, K., Glezer, A., Jagoda, J., "Enhanced Mixing in a Simulated Combustor Using Synthetic Jet Actuators," AIAA Paper 99-0449, Jan. 1999.

Crook, A. and Wood, N. J., "Measurements and Visualizations of Synthetic Jets," AIAA Paper 2001-0145, Jan. 2001.

Crook, A., Sadri, A. M., and Wood, N. J., "The Development and Implementation of Synthetic Jets for the Control of Separated Flow," AIAA Paper 99-3176, July 1999.

Fischer, F. A., Fundamentals of Electroacoustics, Interscience Publishers, Inc., New York, NY, 1955.

Gilarranz, J. L. and Rediniotis, O. K., "Compact, High-Power Synthetic Jet Actuators for Flow Separation Control," AIAA Paper 2001-0737, Jan. 2001.

Honohan, A. M., Amitay, M., and Glezer, A., "Aerodynamic Control Using Synthetic Jets," AIAA Paper 2000-2401, June 2000.

Hunt, F. V., Electroacoustics: The Analysis of Transduction, and Its Historical Background," 2nd Edition, Acoustical Society of America, Woodbury NY, 1982.

Ingard, U., "Acoustic Nonlinearity of an Orifice," *Journal of Acoustic Society of America*, Vol. 42, No. 1, pp. 6-17, 1967.

Kral, L. D., Donovan, J. F., Cain, A. B., and Cary, A. W., "Numerical Simulation of Synthetic Jet Actuators," AIAA Paper 97-1824, June 1997.

Mallinson, S. G., Reizes, J. A., Hong, G., and Haga, H., "The Operation and Application of Synthetic Jet Actuators," AIAA Paper 2000-2402, June 2000.

McCormick D. C, "Boundary Layer Separation Control with Directed Synthetic Jets," AIAA Paper 2000-0519, Jan. 2000.

Mittal, R., Rampuggoon, P., Udaykumar, H. S., "Interaction of a Synthetic Jet with a Flat Plate Boundary Layer," AIAA Paper 2001-2773, June 2001.

Prasad, S., Sankar, B., Cattafesta, L., and Sheplak, M., "Two-Port Electro-Acoustic Model of an Electro-Active Composite Circular Plate," To be presented at the 43rd AIAA/ASME/ASCE/AHS Structures, Structural Dynamics, and Materials Conference, AIAA Paper 2002-599, April 2002.

Rathnasingham, R. and Breuer, K. S., "Coupled Fluid-Structural Characteristics of Actuators for Flow Control," *AIAA Journal*, Vol. 35, No. 5, pp. 832-837, May 1997.

Rizzetta, D. P., Visbal, M. R., and Stanek, M. J., "Numerical Investigation of Synthetic Jet Flowfields," AIAA 98-2910, June 1998.

Rossi, M. , Acoustics and Electroacoustics, Artech House, Norwood, MA, pp. 245-373, 1988.

Sheplak, M., Schmidt, M.A., and Breuer, K.S., "A Wafer-Bonded, Silicon Nitride Membrane Microphone with Dielectrically-Isolated, Single-Crystal Silicon Piezoresistors," Technical Digest, Solid-State Sensor and Actuator Workshop, pp. 23-26, Hilton Head, SC, June 1998.

Smith, B. L. and Glezer, A., "The Formation and Evolution of Synthetic Jets," *Physics of Fluids*, Vol. 10, No. 9, pp. 2281-2297, 1998.

Smith, D. R., Amitay, M., Kibens, V., Parekh, D. E., and Glezer, A., "Modification of Lifting Body Aerodynamics Using Synthetic Jet Actuators, AIAA Paper 98-0209, Jan. 1998.

Utturkar, Y., Mittal, R., Rampunggoon, P., and Cattafesta, L., "Sensitivity of Synthetic Jets to the Design of the Jet Cavity, AIAA Paper 2002-0124, Jan. 2002.

White, F. M., Viscous Flow, McGraw-Hill, Inc. N.Y., pp. 143-148, 1974.

White, F. M., Fluid Mechanics, McGraw-Hill, Inc. N.Y., pp. 377-379, 1979.